DEVELOPMENTAL BIOLOGY

VGLL4 promotes osteoblast differentiation by antagonizing TEADs-inhibited Runx2 transcription

Jinlong Suo[1]*, Xue Feng[1]*, Jiayi Li[2], Jinghui Wang[1], Zuoyun Wang[1†], Lei Zhang[1,3,4†], Weiguo Zou[1,3,4†]

VGLL4 has been identified as a YAP inhibitor. However, the exact function of VGLL4 in bone development and bone homeostasis remains unclear. In this study, we demonstrated that VGLL4 breaks TEADs-mediated transcriptional inhibition of RUNX2 to promote osteoblast differentiation and bone development. We found that knockout of VGLL4 in mesenchymal stem cells and preosteoblasts showed osteoporosis and a cleidocranial dysplasia–like phenotype due to osteoblast differentiation disorders. Mechanistically, we showed that the TEAD transcriptional factors severely inhibited osteoblast differentiation in a YAP binding–independent manner. TEADs interacted with RUNX2 to repress RUNX2 transcriptional activity. Furthermore, VGLL4 relieved the transcriptional inhibition of TEADs by directly competing with RUNX2 to bind TEADs through its two TDU domains. Collectively, our studies demonstrate that VGLL4 plays an important role in regulating osteoblast differentiation and bone development, and that TEADs regulate the transcriptional activity of RUNX2, which may shed light on treatment of cleidocranial dysplasia and osteoporosis.

INTRODUCTION

Cleidocranial dysplasia (CCD) is a hereditary disease characterized by incomplete closure of the fontanelle, abnormal clavicle, short stature, and skeletal dysplasia. It has been reported that there are multiple *Runx2* mutations in human CCD syndrome (*1*, *2*). Mature osteoblasts defect and bone mineralization disorders were observed in *Runx2*-deficient mice. The *Runx2*-heterozygous mice show similar phenotypes to the CCD syndrome (*2*–*4*). RUNX2 triggers mesenchymal stem cells (MSCs) to differentiate into osteoblasts (*3*, *5*). According to the skeletal pathology studies in humans and mice, it is important to accurately regulate *Runx2* activity during bone formation and bone remodeling (*6*, *7*). However, the molecular regulation of *Runx2* activity remains to be further studied.

The evolutionarily conserved Hippo pathway is essential for tissue growth, organ size control, and cancer development (*8*–*11*). Numerous evidences revealed the important roles of Hippo components in regulating bone development and bone remodeling. YAP, the essential downstream effector of Hippo pathway, regulates multiple steps of chondrocyte differentiation during skeletal development and bone repair (*12*). YAP also promotes osteogenesis and suppresses adipogenic differentiation by regulating β-catenin signaling (*13*). VGLL4, a member of the Vestigial-like family, acts as a transcriptional repressor of YAP-TEADs in the Hippo pathway (*14*). Our previous work found that VGLL4 suppressed lung cancer and gastric cancer progression by directly competing with YAP to bind TEADs through its two TDU (Tondu) domains (*9*, *15*). We also found that VGLL4 played a critical role in heart valve development by regulating heart valve remodeling, maturation, and homeostasis (*16*). Moreover, our team found that VGLL4 regulated muscle regeneration in YAP-dependent manner at the proliferation stage and YAP-independent manner at the differentiation stage (*17*). Our previous studies suggest that VGLL4 plays an important role to regulate cell differentiation in multiple organs. However, the function of VGLL4 in skeletal formation and bone remodeling is unknown.

Here, we reveal the function of VGLL4 in osteoblast differentiation and bone development. Our in vivo data show that global knockout of *Vgll4* results in a wide variety of skeletal defects similar to *Runx2* heterozygote mice. Our in vitro studies reveal that VGLL4 deficiency strongly inhibits osteoblast differentiation. We further demonstrate that TEADs can bind to RUNX2, thereby inhibiting the transcriptional activity of RUNX2 independent of YAP binding. VGLL4 could relieve the inhibitory function of TEADs by breaking its interaction with RUNX2. In addition, deletion of VGLL4 in MSCs shows similar skeletal defects with the global *Vgll4*-deficient mice. Further studies show that knocking down TEADs or overexpressing RUNX2 in VGLL4-deficient osteoblasts reverses the inhibition of osteoblast differentiation.

RESULTS

VGLL4 deficiency impairs bone ossification

To study the function of VGLL4 in bone, we first measured β-galactosidase activity in $Vgll4^{LacZ/+}$ mice (*16*). β-Galactosidase activity was enriched in trabecular bones, cortical bones, cranial suture, and calvaria cultures (fig. S1, A to C). Furthermore, in bone marrow MSCs (BMSCs), $Vgll4^{LacZ/+}$ mice displayed β-galactosidase activity in osteoblast-like cells (fig. S1D). During osteoblast differentiation in vitro, osteoblast marker genes such as alkaline phosphatase (*Alp*) and Sp7 transcription factor (*Osterix*) were increased and peaked at day 7. *Vgll4* showed similar trend in this process at both mRNA and protein levels (Fig. 1A and fig. S1, E and F). To further clarify the important role of VGLL4 in bone development, we used a $Vgll4^{Vgll4\text{-}eGFP/+}$ reporter mouse line in which VGLL4–enhanced green fluorescent protein (eGFP) fusion protein expression is under the control of the endogenous

[1]State Key Laboratory of Cell Biology, Shanghai Institute of Biochemistry and Cell Biology, Center for Excellence in Molecular Cell Science, Chinese Academy of Sciences; University of Chinese Academy of Sciences, Shanghai 200031, China. [2]Department of Laboratory Medicine, Shanghai University of Medicine & Health Sciences Affiliated Zhoupu Hospital, Shanghai 201318, China. [3]School of Life Science and Technology, ShanghaiTech University, 100 Haike Road, Shanghai 201210, China. [4]Bio-Research Innovation Center, Shanghai Institute of Biochemistry and Cell Biology, Chinese Academy of Sciences, Suzhou 215121, China.
*These authors contributed equally to this work.
†Corresponding author. Email: zouwg94@sibcb.ac.cn (W.Z.); rayzhang@sibcb.ac.cn (L.Z.); wangzuoyun@sibcb.ac.cn (Z.W.)

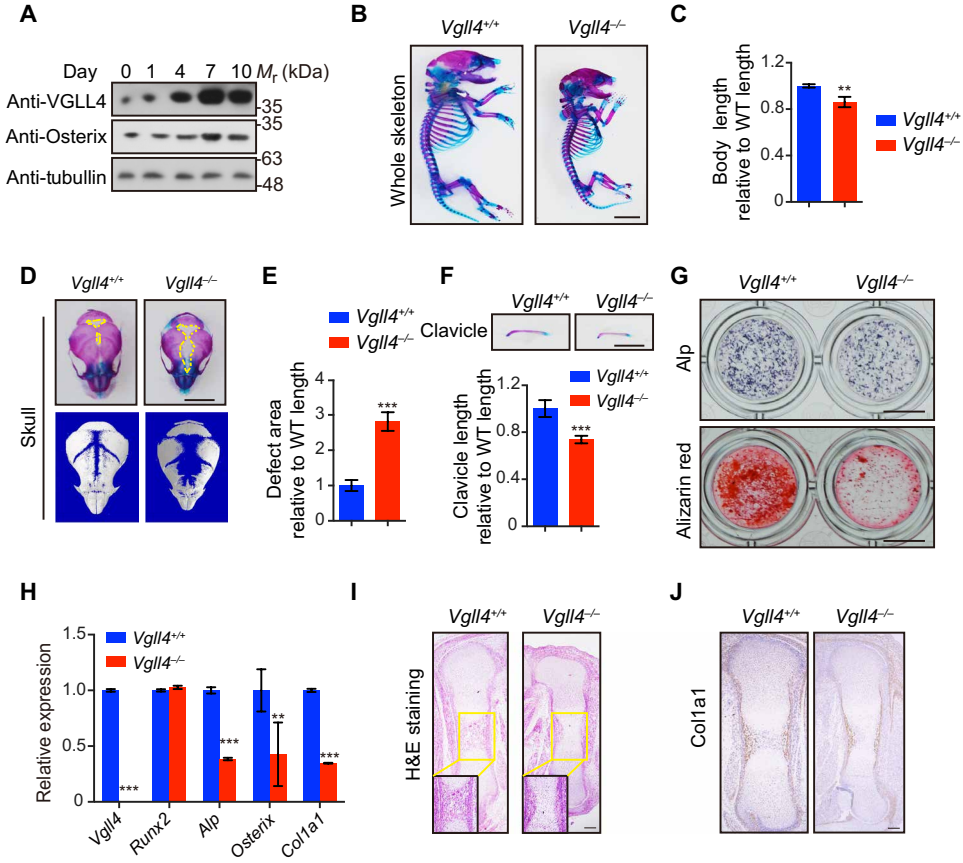

Fig. 1. Deletion of *Vgll4* causes abnormal bone development. (**A**) Immunoblotting showed the expression profile of VGLL4 during osteoblast differentiation in C57BL/6J mouse BMSCs. Samples were collected at 0, 1, 4, 7, and 10 days after differentiation. (**B**) Skeletons of WT and *Vgll4*$^{-/-}$ mice at postnatal day 1 (P1) were double-stained by Alizarin red/Alcian blue ($n = 5$). Scale bar, 5 mm. (**C**) Quantification of body length in (B). (**D**) Skull preparations from control and *Vgll4*$^{-/-}$ mouse newborns were double-stained with Alizarin red and Alcian blue at P1. μ-QCT images of skulls were taken from control and *Vgll4*$^{-/-}$ mice at P4. Scale bar, 5 mm. (**E**) Quantification of skull defect area in (D). (**F**) Clavicle preparations from control and *Vgll4*$^{-/-}$ mouse newborns were double-stained with Alizarin red and Alcian blue at P1 and quantification of clavicle length. Scale bar, 5 mm. (**G**) Alp staining and Alizarin red staining of calvarial cells from WT and *Vgll4*$^{-/-}$ mice after cultured in osteogenic medium. Scale bar, 3 mm. (**H**) Relative mRNA levels were quantified by RT-PCR. (**I**) Hematoxylin and eosin (H&E) staining of femur from WT and *Vgll4*$^{-/-}$ mice at embryonic day 16.5. Scale bar, 125 μm. (**J**) In situ hybridization for *Col1α1* immunostaining. Scale bar, 125 μm. In (C), (E), (F), and (H), data were presented as means ± SEM; *$P < 0.05$, **$P < 0.01$, and ***$P < 0.001$, ns, no significance; unpaired Student's *t* test. Photo credit: Jinlong Suo, State Key Laboratory of Cell Biology, Shanghai Institute of Biochemistry and Cell Biology, Center for Excellence in Molecular Cell Science, Chinese Academy of Sciences; University of Chinese Academy of Sciences, Shanghai.

VGLL4 promoter, and GFP staining reflects VGLL4 expression pattern in skeletal tissues (*16*). GFP staining was performed at embryonic day 18.5, week 1, week 2, and week 4 stages. The results indicated that the VGLL4 expression level was increased during bone development (fig. S1G). In addition, VGLL4 was enriched in trabecular bones, cortical bones, chondrocytes, cranial suture, and calvaria (fig. S1, G and K to M). We then observed the colocalization of VGLL4-eGFP with markers of MSCs (CD105), osteoblasts [osteocalcin (OCN)], and chondrocytes [collagen 2a1 (Col2a1)] in long bone and calvaria (fig. S1, H to M). Next, we analyzed VGLL4 expression pattern during osteoblast development in vivo (fig. S1N), which was similar to *Alp* and *Osterix* expression patterns in mouse BMSCs of different ages. Together, both in vivo and in vitro data suggest that VGLL4 may play roles in osteoblast differentiation and bone development.

To investigate the potential function of VGLL4 in bone, we next analyzed the phenotype of *Vgll4* knockout (*Vgll4*$^{-/-}$) mice (*16*). The newborn *Vgll4* knockout mice were significantly smaller and underweight compared with their control littermates (Fig. 1, B and C, and fig. S2, A and B). In particular, the membranous ossification of the skull was impaired in *Vgll4*$^{-/-}$ newborns compared with the control littermates (Fig. 1, D and E). Furthermore, *Vgll4* knockout mice developed a marked dwarfism phenotype with short legs and short clavicles (Fig. 1, C and F). To assess the role of VGLL4 in osteoblast differentiation, calvarial cells from *Vgll4*$^{-/-}$ mice and wild-type (WT) mice were cultured in osteogenic medium. The activity of *Alp* in the *Vgll4* deletion group was significantly reduced at the seventh day of differentiation (Fig. 1G, top) and was markedly weakened over a 14-day culture period as revealed by Alizarin red S staining (Fig. 1G, bottom). The declined osteogenesis in *Vgll4* knockout cells was confirmed by the decreased expression of a series of osteogenic marker genes (Fig. 1H), including *Alp*, *Osterix*, and collagen type1 α1 (*Col1α1*). In addition, in *Vgll4*$^{-/-}$ mice, bone development was severely impaired with remarkable decrease in bone length and almost a complete loss of bone ossification (Fig. 1I). Consistently, immunohistochemical analysis of bone tissue sections from embryos

at embryonic day 14.5 further confirmed the defects of bone formation and impaired osteoblast differentiation in *Vgll4*$^{-/-}$ mice (Fig. 1J). Together, our study suggests that VGLL4 is likely to regulate MSC fate by enhancing osteoblast differentiation.

Given that the smaller size of mice is often caused by dysplasia, we also paid attention to the development of cartilage after *Vgll4* deletion. As we expected, cartilage development was delayed in *Vgll4*-deficient mice determined by Safranin O (SO) staining (fig. S2C). Immunohistochemical analysis of collagen X (Col X) further confirmed the delay of cartilage development in *Vgll4*$^{-/-}$ mice (fig. S2D). However, additional experiments would be required to determine the regulatory mechanism behind the observed chondrodysplasia. Although dwarfism was observed and trabecular bones were significantly reduced in the adult *Vgll4*$^{-/-}$ mice, no significant cartilage disorder was observed by SO staining (fig. S2E). In adults, bone is undergoing continuous bone remodeling, which involves bone formation by osteoblasts and bone resorption by osteoclasts. We speculated that *Vgll4* deletion might lead to decreased osteoclast activity. To distinguish this possibility, we performed histological analysis by tartrate-resistant acid phosphatase (TRAP) staining to detect osteoclast activity. The results showed that osteoclast activity was comparable between *Vgll4*$^{-/-}$ mice and their control littermates (fig. S2F). Together, our results suggest that the phenotypes observed in *Vgll4*$^{-/-}$ mice are mainly due to the defect of osteoblast activity.

MSC-specific deletion of *Vgll4* leads to abnormal ossification

To further explore the role of *Vgll4* in the commitment of MSCs to the fate of osteoblasts, we generated *Prx1-cre; Vgll4*$^{floxp/floxp}$ mice (hereafter *Vgll4*^{prx1} mice) (fig. S3A). *Prx1-Cre* activity is mainly restricted to limbs and craniofacial mesenchyme cells (*18*, *19*). Western blot analysis confirmed that VGLL4 was knocked out in BMSCs (fig. S3B). *Vgll4*^{prx1} mice survived normally after birth and had normal fertility. However, *Vgll4*^{prx1} mice exhibited marked dwarfism that was independent of sex (Fig. 2, A and B, and fig. S3C), which was similar to the phenotype of *Vgll4*$^{-/-}$ mice. In particular, the membranous ossification of the skull and clavicle was also impaired in *Vgll4*^{prx1} mouse newborns compared with control littermates (Fig. 2, C to E). To assess the role of VGLL4 in osteoblast differentiation, BMSCs from *Vgll4*^{prx1} and *Vgll4*$^{fl/fl}$ mice were cultured in osteogenic medium. Markedly decreased ALP activity and mineralization were observed in *Vgll4*^{prx1} mice (Fig. 2, F and G). The declined osteogenesis in *Vgll4* knockout osteoblasts was also proved by the decreased expression of a series of osteogenic marker genes, including *Alp*, *Osterix*, and *Col1a1* (Fig. 2H). Normal *Runx2* expression was detected in *Vgll4*^{prx1} mice (Fig. 2H). To further verify the role of VGLL4 in osteoblast differentiation, BMSCs from *Vgll4*$^{fl/fl}$ mice were infected with GFP and Cre recombinase (Cre) lentivirus and then cultured in osteogenic medium. *Vgll4*$^{fl/fl}$ BMSCs infected with Cre lentivirus showed markedly decreased ALP activity and mineralization (fig. S4A). Reduced VGLL4 expression by Cre lentivirus was confirmed by reverse transcription polymerase chain reaction (RT-PCR) (fig. S4B). The declined osteogenesis was also proved by the decreased expression of a series of osteogenic marker genes, including *Alp*, *Osterix*, and *Col1a1* (fig. S4B).

We next performed PCNA (proliferating cell nuclear antigen) staining and MTT assay to detect whether VGLL4 influences cell proliferation during bone development. No significant differences were found after VGLL4 deletion (fig. S5, A to C). We also did not detect significant changes of proliferation-related genes and YAP downstream genes (fig. S5, D and E). We next performed TUNEL (terminal deoxynucleotidyl transferase–mediated deoxyuridine triphosphate nick end labeling) staining to detect whether VGLL4 influences cell apoptosis. In addition, no significant differences were found after VGLL4 deletion (fig. S5, F and G).

To further determine the function of VGLL4 in skeletal system, we did micro-quantitative computed tomography (μ-QCT) analysis to compare the changes in bone-related elements in the long bones of *Vgll4*^{prx1} mice and control littermates. We found that the 3-month-old *Vgll4*^{prx1} mice showed decreased bone mass per tissue volume (BV/TV) relative to age-matched control littermates (Fig. 2, I and J). Further analysis showed a reduction in trabecular number (Tb.N) of *Vgll4*^{prx1} mice compared to control mice (Fig. 2K), which was accompanied by a decrease in trabecular thickness (Tb.Th) and an increase in trabecular separation (Tb.Sp) compared to control mice (Fig. 2, L and M). *Vgll4*^{prx1} mice also showed decreased cortical bone thickness (Cor.Th) relative to the *Vgll4*$^{fl/fl}$ mice (Fig. 2N). The von Kossa staining showed reduced bone mineral deposition in 3-month-old *Vgll4*^{prx1} mice (Fig. 2O). The mineral apposition rate (MAR) was also decreased in *Vgll4*^{prx1} mice compared with control littermates by fluorescent double labeling of the mineralizing front (Fig. 2, P and Q). Consistent with the decreased bone mass in *Vgll4*^{prx1} mice, the enzyme-linked immunosorbent assay (ELISA) assay of N-terminal propeptide of type I procollagen (PINP), a marker of bone formation, revealed a reduced bone formation rate in *Vgll4*^{prx1} mice (Fig. 2R). However, the ELISA assay of C-terminal telopeptide of collagen type 1 (CTX-1), a marker of bone resorption, showed that the bone resorption rate of *Vgll4*^{prx1} mice did not change significantly (Fig. 2S). Collectively, *Vgll4* conditional knockout mice mimicked the main phenotypes of the global *Vgll4* knockout mice, further indicating that VGLL4 specifically regulates bone mass by promoting osteoblast differentiation.

Preosteoblast-specific deletion of *Vgll4* reduced bone formation

To further determine whether the abnormal osteogenesis in *Vgll4*^{prx1} mice was caused by a primary defect in osteoblast development, we generated an osteoblast-specific *Osx-cre; Vgll4*$^{floxp/floxp}$ mice (hereafter *Vgll4*^{Osx} mice) by crossing *Vgll4*$^{fl/fl}$ mice with *Osx-Cre* mice, a line in which Cre expression is primarily restricted to osteoblast precursors (fig. S6A) (*6*, *20*). *Vgll4*^{Osx} mice survived normally after birth and had normal fertility, but exhibited marked dwarfism in comparison with *Osx-Cre* mice (fig. S6, B and C), which was similar to the phenotypes of *Vgll4*$^{-/-}$ and *Vgll4*^{prx1} mice. In addition, the membranous ossification of the skull and clavicle was also impaired in *Vgll4*^{Osx} mice compared with control littermates (fig. S6C). μ-QCT analysis further confirmed the osteogenic phenotype of *Vgll4*^{Osx} mice (fig. S6, D to J). Hence, the *Vgll4*^{Osx} mice summarized the defects observed in the *Vgll4*^{prx1} mice, thus supporting the conclusion that VGLL4 is necessary for the differentiation and function of committed osteoblast precursors.

TEADs interacts with RUNX2 and impairs osteoblast differentiation

We next worked to figure out the mechanism how VGLL4 controls bone mass and osteoblast differentiation. The pygmy and cranial closure disorders in *Vgll4*$^{-/-}$ mice were similar to that of *Runx2*-heterozygous mice. We therefore examined the potential interaction

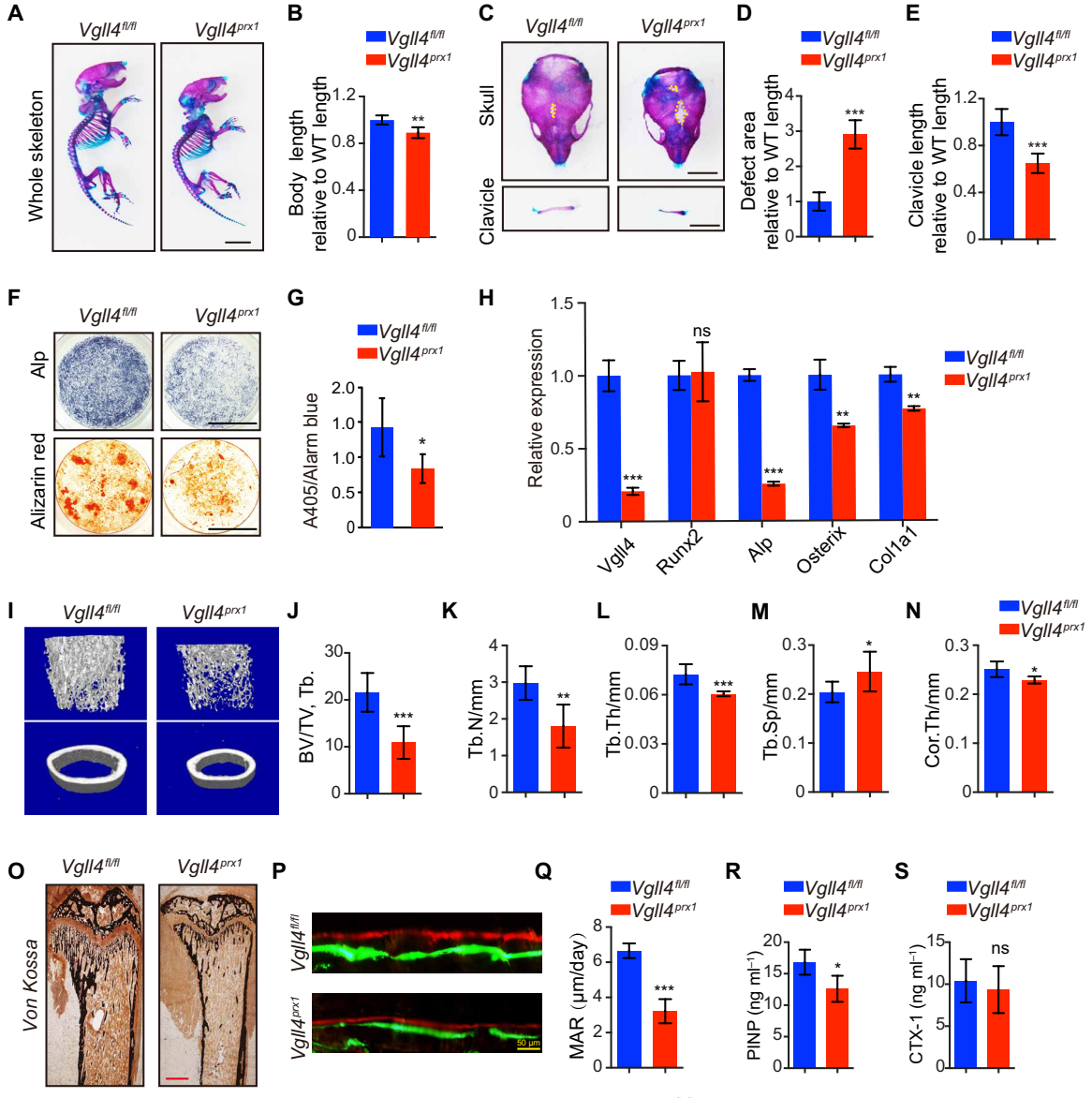

Fig. 2. Inactivation of VGLL4 in MSCs leads to impaired bone ossification. (**A**) Skeletons of *Vgll4*$^{fl/fl}$ *and Vgll4*^{prx1} mice at P1 were double-stained by Alizarin red and Alcian blue. Scale bar, 5 mm. (**B**) Quantification of body length in (A) ($n = 6$). (**C**) Skull and clavicle preparation from *Vgll4*$^{fl/fl}$ and *Vgll4*^{prx1} mouse newborns were double-stained with Alizarin red and Alcian blue at P1. Scale bars, 5 mm. (**D**) Quantification of the defect area of skulls in (C) ($n = 6$). (**E**) Quantification of clavicle length in (C) ($n = 6$). (**F**) Alp staining and Alizarin red staining of BMSCs from *Vgll4*$^{fl/fl}$ and *Vgll4*^{prx1} mice after cultured in osteogenic medium. Scale bars, 3 mm. (**G**) Alp activity was measured by phosphatase substrate assay. (**H**) Relative mRNA levels were quantified by RT-PCR. (**I**) 3D μ-QCT images of trabecular bone (top) and cortical bone (bottom) of distal femurs. (**J** to **N**) μ-QCT analysis for trabecular bone volume per tissue volume (BV/TV, Tb) (J), trabecular number (Tb.N/mm) (K), trabecular thickness (Tb.Th/mm) (L), trabecular separation (Tb.Sp/mm) (M), and cortical bone thickness (Cor.Th/mm) (N). (**O**) Representative images of von Kossa staining of 12-week-old *Vgll4*$^{fl/fl}$ and *Vgll4*^{prx1} mice. Scale bar, 500 μm. (**P**) Representative images of calcein and Alizarin red S labeling of proximal tibia. Scale bar, 50 μm. (**Q**) Quantification of MAR. (**R** and **S**) ELISA analysis of serum PINP (ng ml^{-1}) and CTX-1 (ng ml^{-1}) from 10-week-old *Vgll4*$^{fl/fl}$ and *Vgll4*^{prx1} mice ($n = 5$). In (B), (D), (E), (G), (H), (J) to (N), and (Q) to (S), data were presented as means ± SEM; *$P < 0.05$, **$P < 0.01$, and ***$P < 0.001$; ns, no significance; unpaired Student's *t* test. Photo credit: Jinlong Suo, State Key Laboratory of Cell Biology, Shanghai Institute of Biochemistry and Cell Biology, Center for Excellence in Molecular Cell Science, Chinese Academy of Sciences; University of Chinese Academy of Sciences, Shanghai.

between VGLL4 and RUNX2. However, coimmunoprecipitation experiments did not show the interaction between VGLL4 and RUNX2 (Fig. 3A). Previous studies showed that VGLL4 could compete with YAP for binding to TEADs (*9*). The TEAD family contains four highly homologous proteins (*8*), which is involved in the regulation of myoblast differentiation and muscle regeneration (*21*). We determined whether the binding of VGLL4 with RUNX2 requires TEADs. Coimmunoprecipitation experiments showed that RUNX2 and TEAD1–4 had almost equivalent interactions (Fig. 3B). Next, we investigated whether TEADs control the transcriptional activity of *Runx2*. We used the 6xOSE2-luciferase reporter system that is specifically activated by RUNX2 to verify the role of TEADs

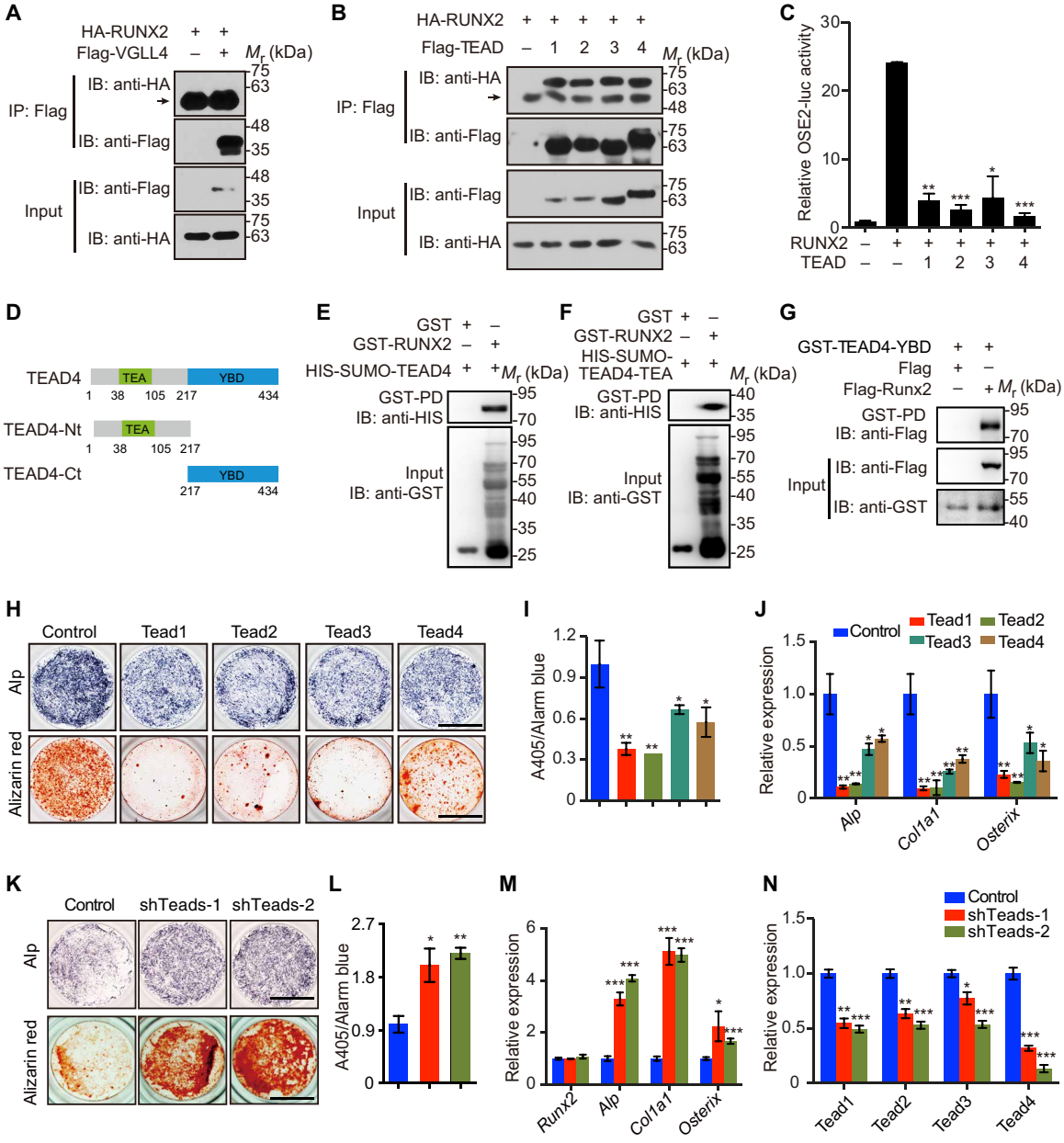

Fig. 3. TEADs deficiency impaired osteoblast differentiation. (**A**) Coimmunoprecipitation experiments of RUNX2 and VGLL4 in HEK-293T cells. The arrow indicated IgG heavy chain. (**B**) Coimmunoprecipitation experiments of RUNX2 and TEAD1–4 in HEK-293T cells. The arrow indicated IgG heavy chain. (**C**) 6xOSE2-luciferase activity was determined in C3H10T1/2 cells cotransfected with RUNX2 and TEAD1–4. Data were calculated from three independent replicates. (**D**) Schematic illustration of the domain organization for TEAD4, TEAD4-Nt, and TEAD4-Ct. (**E**) GST pull-down (PD) analysis between purified GST-RUNX2 and HIS-SUMO-TEAD4 proteins. (**F**) GST pull-down analysis between purified GST-RUNX2 and HIS-SUMO-TEAD4-TEA proteins. (**G**) Lysates from HEK-293T cells with Flag and Flag-RUNX2 expressions were incubated with recombinant GST-TEAD4-YBD protein. GST pull-down assay showed the binding between RUNX2 and TEAD4-YBD. (**H**) Cells isolated from WT mice were infected with TEAD lentivirus. Osteoblast differentiation was evaluated by Alp staining and Alizarin red staining after culture in osteoblast differentiation medium for 7 days (top) and 14 days (bottom). Data are representative of three independent experiments. Scale bars, 3 mm. (**I**) Alp activity quantification was measured by phosphatase substrate assay ($n = 3$). (**J**) Relative mRNA levels of *Alp*, *Col1α1*, and *Osterix* were quantified by RT-PCR. (**K**) Cells isolated from WT mice were infected with TEAD shRNA lentivirus. Osteoblast differentiation was evaluated by Alp staining and Alizarin red staining after culture in osteoblast differentiation medium for 7 days (top) and 14 days (bottom). Data are representative of three independent experiments. Scale bars, 3 mm. (**L**) Alp activity quantification was measured by phosphatase substrate assay ($n = 3$). (**M**) Relative mRNA levels of *Runx2*, *Alp*, *Col1α1*, and *Osterix* were quantified by RT-PCR. (**N**) Relative mRNA levels of *Tead1-4* were quantified by RT-PCR. In (C), (I), (J), and (L) to (N), data were presented as means ± SEM; $^*P < 0.05$, $^{**}P < 0.01$, and $^{***}P < 0.001$; ns, no significance; unpaired Student's *t* test.

(*22*). We performed dual-luciferase reporter assay with 6xOSE2-luciferase and Renilla in C3H10T1/2 cells, and the results showed that TEAD1–4 significantly inhibited the activation of 6xOSE2-luciferase induced by RUNX2 (Fig. 3C). Consistently, knockdown of TEADs by small interfering RNAs (siRNAs) markedly enhanced both basic and RUNX2-induced 6xOSE2-luciferase activity (fig. S8A). TEAD family is highly conserved, which consists of an N-terminal TEA domain and a C-terminal YAP-binding domain (YBD) (Fig. 3D) (*23*). Glutathione *S*-transferase (GST) pull-down assay revealed the direct interaction between RUNX2 and TEAD4 (Fig. 3E). Moreover, both TEA and YBD domains of TEAD4 could bind to RUNX2 (Fig. 3, F and G).

To determine whether overexpression of TEAD1–4 affects osteoblast differentiation, BMSCs from WT mice were infected with TEAD1–4 lentivirus and then cultured in osteogenic medium. The activities of ALP in TEAD1–4 overexpression groups were significantly reduced at the seventh day of differentiation [Fig. 3, H (top) and I] and were significantly weakened by Alizarin red S staining over a 14-day culture period (Fig. 3H, bottom). The declined osteogenesis in TEAD1–4 overexpression cells was confirmed again by the decreased expression of a series of osteogenic marker genes, including *Alp*, *Col1α1*, and *Osterix* (Fig. 3J). Next, we blocked the total activities of TEAD1–4 by short hairpin RNA (shRNA) lentiviral infection (Fig. 3N). The activity of Alp in TEAD1–4 knockdown group was significantly increased [Fig. 3, K (top) and L]. Over a 14-day culture period, osteogenic differentiation was significantly enhanced by Alizarin red S staining (Fig. 3K, bottom). The enhanced osteogenesis in TEAD1–4 knockdown cells was further confirmed by elevated expression of a series of osteogenic marker genes, including *Alp*, *Col1α1*, and *Osterix* (Fig. 3M). These results suggest that TEAD1–4 act as repressors of RUNX2 to inhibit osteoblast differentiation.

VGLL4 promotes osteoblast differentiation by antagonizing with TEADs for RUNX2 binding

To investigate the mechanistic role of VGLL4 in inhibiting osteoblast differentiation, we then verified whether VGLL4 could affect the interaction between TEADs and RUNX2. We found that VGLL4 reduced the interaction between RUNX2 and TEADs (Fig. 4A). To further illustrate the relationship between RUNX2/TEADs/VGLL4, we checked the interaction between RUNX2 and TEADs in the BMSC of *Vgll4*$^{fl/fl}$ mice treated with GFP or Cre lentivirus. We found that the interaction between RUNX2 and TEADs was enhanced in Cre-treated cells (Fig. 4B). We noticed that there were conserved binding sites of RUNX2 (5′-AACCAC-3′) and TEAD (5′-CATTCC-3′) in the promoter regions of *Alpi*, *Osx*, and *Col1a1*, which are three target genes of RUNX2 (*17*, *24*). We performed TEAD4 and RUNX2 chromatin immunoprecipitation (ChIP) assays in BMSCs. The results indicated that both TEAD4 and RUNX2 bound on *Alp*, *Osx*, and *Col1a1* promoters (fig. S7, A to I). VGLL4 was a transcriptional cofactor, which could not bind DNA directly. We have demonstrated that VGLL4 promoted RUNX2 activity by competing for its binding to TEADs. Consistently, VGLL4 partially blocked TEADs-repressed transcriptional activity of RUNX2 (Fig. 4C). However, overexpression of VGLL4 in TEADs knockdown cells showed no marked change on RUNX2-induced 6xOSE2-luciferase activity compared with TEAD knockdown (fig. S8B). We then asked whether loss of VGLL4-induced disorders of osteoblast differentiation is related to TEADs. We knocked down TEADs by lentiviral infection in *Vgll4*-deficient BMSCs and then induced these cells for osteogenic differentiation. The differentiation disorders caused by VGLL4 deletion were restored after TEAD knockdown (Fig. 4, D to F). These data supported that VGLL4 released the inhibition of TEADs on RUNX2, thereby promoting osteoblast differentiation.

TEADs regulate RUNX2 activity independent of YAP-binding

YAP, the key transcription cofactor in the Hippo pathway, has been widely reported in regulating bone development and bone mass (*12*, *13*). VGLL4, a previously identified YAP antagonist, directly competes with YAP for binding to TEADs (*9*). Therefore, we suspected that the inhibition of RUNX2 transcriptional activity caused by VGLL4 deletion might be dependent on YAP. To this end, we validated the role of YAP by 6xOSE2-luciferase reporter system. The data showed that YAP promoted RUNX2 activity in a dose-dependent manner (Fig. 5A). Moreover, TEAD4 significantly inhibited 6xOSE2-luciferase activity induced by YAP (Fig. 5B). TEAD4^{Y429H}, a mutation that impairs the interaction between TEAD4 and YAP/TAZ (Fig. 5C) (*25*), did not promote 3xSd-luciferase activity induced by YAP (Fig. 5D). We found that both TEAD and TEAD4^{Y429H} could interact with RUNX2 (Fig. 5E), and both TEAD4 and TEAD4^{Y429H} could inhibit the activity of RUNX2 in a dose-dependent manner (Fig. 5, F and G). Restoring the expression of both TEAD4 and TEAD4^{Y429H} could reverse the increased osteoblast differentiation in TEAD knockdown BMSCs (Fig. 5, H and I). Furthermore, overexpression of TEAD1 could further inhibit osteogenic differentiation of BMSCs after YAP knockdown (Fig. 5J). Together, these data suggest that the inhibition of RUNX2 activity by TEADs is independent of YAP binding.

RUNX2 rescues the osteogenesis differentiation defects due to *Vgll4* deletion

We next examined how VGLL4 breaks the interaction between RUNX2 and TEADs. It has been reported that VGLL4 relies on its own two TDU domains to interact with TEADs (*9*), and VGLL4 HF4A mutation can disrupt the interaction between VGLL4 and TEADs (*15*). We hypothesized that VGLL4 competes with RUNX2 for TEAD1 binding depending on its TDU domain. On the basis of these previous studies, we performed coimmunoprecipitation experiments and found that VGLL4 HF4A abolished the interaction between VGLL4 and TEAD1 but did not affect the interaction between TEAD1 and RUNX2 (Fig. 6A). VGLL4 partially rescued the inhibition of RUNX2 transcriptional activity by TEAD1; however, VGLL4 HF4A lost this function (Fig. 6B). We then overexpressed TEAD1 by lentivirus infection in primary calvarial cells and found that the transcriptional level of *Alp* was significantly inhibited. This inhibition was released by overexpressing VGLL4 but not VGLL4 HF4A (Fig. 6C). To further verify the specific regulation of RUNX2 activity by VGLL4, we performed a coimmunoprecipitation experiment with low and high doses of VGLL4 and VGLL4 HF4A. The results showed that the TEAD1-RUNX2 interaction was gradually repressed along with an increasing dose of VGLL4 but not VGLL4 HF4A (Fig. 6D). Similarly, the inhibition of RUNX2 transcriptional activity by TEAD1 was gradually released with an increasing dose of VGLL4 but not VGLL4 HF4A (Fig. 6E). Super-TDU, a peptide mimicking VGLL4, could also reduce the interaction between purified RUNX2 and TEAD4 proteins (Fig.6F). Thus, these findings suggest that VGLL4 TDU domain competes with RUNX2 for TEADs binding to release RUNX2 transcriptional activity.

Furthermore, we overexpressed RUNX2 by lentivirus infection in *Vgll4* knockout BMSCs during osteogenic differentiation, and we

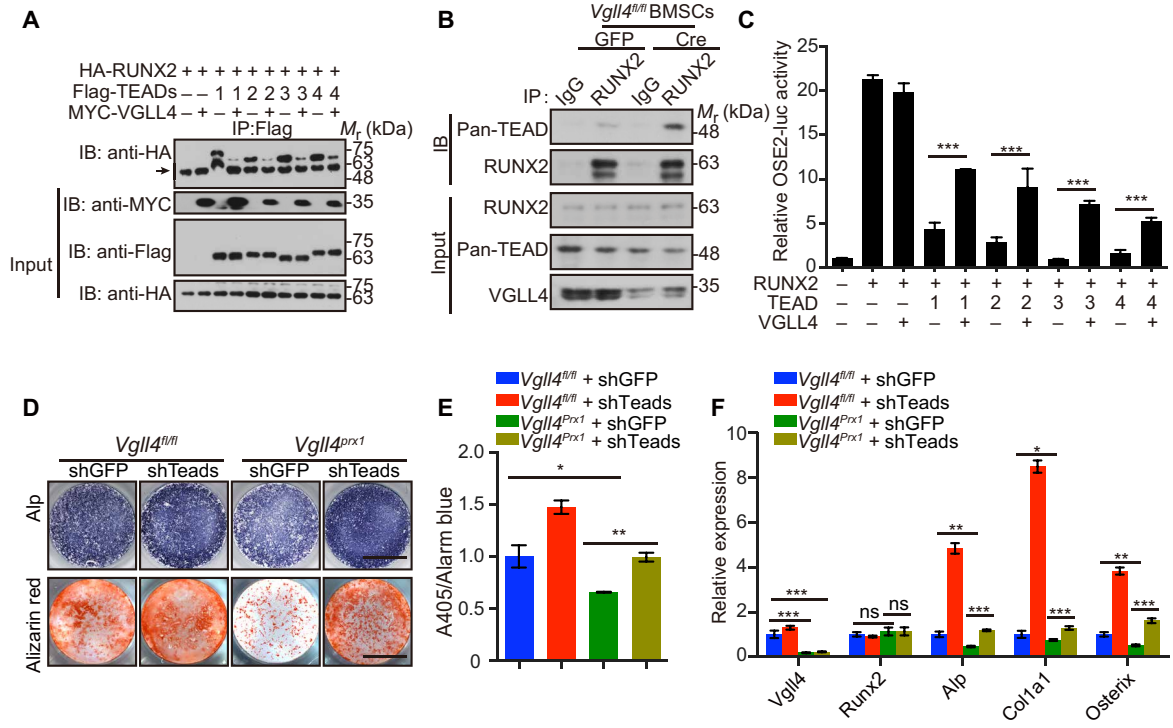

Fig. 4. VGLL4 promotes RUNX2 activity by competing for its binding to TEADs. (**A**) Coimmunoprecipitation experiments of RUNX2, TEADs, and VGLL4 in HEK-293T cells. The arrow indicated IgG heavy chain. (**B**) Coimmunoprecipitation experiments of RUNX2 and TEADs in BMSCs cells of *Vgll4*$^{fl/fl}$ mice treated with GFP and Cre lentivirus. (**C**) 6xOSE2-luciferase activity was determined in C3H10T1/2 cells cotransfected with RUNX2, TEADs, and VGLL4. (**D**) Cells isolated from *Vgll4*$^{fl/fl}$ and *Vgll4*^{prx1} mice were infected with GFP and TEAD shRNA lentivirus. Osteoblast differentiation was evaluated by Alp staining and Alizarin red staining after culture in osteoblast differentiation medium for 7 days (top) and 14 days (bottom). Data are representative of three independent experiments. Scale bars, 3 mm. (**E**) Alp activity quantification was measured by phosphatase substrate assay ($n = 3$). (**F**) Relative mRNA levels of *Vgll4*, *Runx2*, *Alp*, *Col1α1*, and *Osterix* were quantified by RT-PCR. In (B), (D), and (E), data were presented as means ± SEM; *$P < 0.05$, **$P < 0.01$, and ***$P < 0.001$; ns, no significance; unpaired Student's *t* test.

found that RUNX2 could significantly restore the osteogenic differentiation disorder caused by *Vgll4* deletion (Fig. 6, G to I). Together, these data suggest a genetic interaction between VGLL4/TEADs/RUNX2 and provide evidences that RUNX2 overexpression rescues osteogenic differentiation disorders caused by VGLL4 deletion.

Collectively, our study demonstrates the important roles of VGLL4 in osteoblast differentiation, bone development, and bone homeostasis. In the early stage of osteoblast differentiation, TEADs interact with RUNX2 to inhibit its transcriptional activity in a YAP binding–independent manner. During differentiation progress, VGLL4 expression gradually increases to dissociate the interaction between TEADs and RUNX2, thereby releasing the inhibition of RUNX2 transcriptional activity by TEADs and promoting osteoblasts differentiation (Fig. 6J).

DISCUSSION

Accumulating evidences have suggested that the Hippo pathway plays key roles in regulating organ size and tissue homeostasis (*8*, *10*). However, the transcription factors TEADs have not been reported in skeletal development and bone-related diseases. VGLL4 functions as a new tumor suppressor gene, which has been reported to negatively regulate the YAP-TEADs transcriptional complex. Our previous studies show that VGLL4 plays important roles in many tissue homeostasis and organ development, such as heart and muscle (*16*, *17*). In this study, we provide evidences to show that VGLL4 can break TEADs-mediated transcriptional inhibition of RUNX2 to promote osteoblast differentiation and bone development independent of YAP binding.

Overall, our studies establish the *Vgll4*-specific knockout mouse model in the skeletal system. We show that VGLL4 deletion in MSCs leads to abnormal osteogenic differentiation with delayed skull closure and reduced bone mass. Our data also reveal that VGLL4 deletion leads to chondrodysplasia. Recent researches identified that chondrocytes have the ability to transdifferentiate into osteoblasts (*26*–*28*), suggesting the possibility that loss of VGLL4 might reduce or delay the pool of chondrocytes that differentiate into osteoblasts. We identify that VGLL4 regulates the RUNX2-TEADs transcriptional complex to control osteoblast differentiation and bone development. TEADs can bind to RUNX2 and inhibit its transcriptional activity in a YAP binding–independent manner. Recent studies pointed out that reciprocal stabilization of ABL and TAZ regulates osteoblastogenesis through transcription factor RUNX2 (*29*); however, we found that TEAD4-Y429H, a mutation at the binding site of TAZ and TEAD (*25*, *30*, *31*), can still significantly inhibit the activity of RUNX2. Therefore, we consider that the way TEAD regulates RUNX2 may not depend on TAZ regulation. Further research found that VGLL4, but not VGLL4 HF4A, can alleviate the inhibition by influencing the binding between RUNX2 and TEADs. It is possible that VGLL4 might influence the structure organization

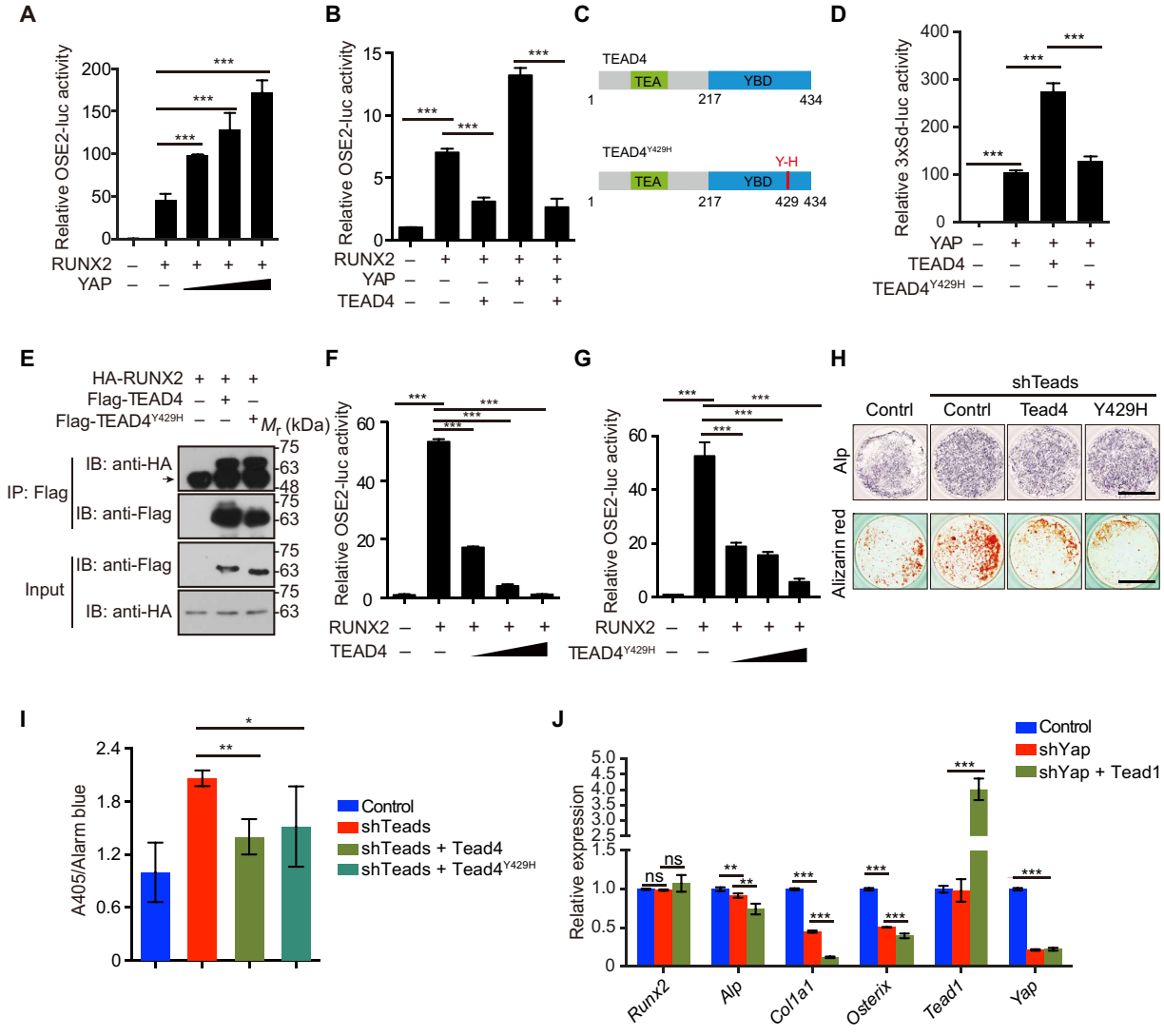

Fig. 5. TEADs inhibit RUNX2 activity independent of YAP binding. (**A**) Effects of YAP on Runx2-activated 6xOSE2-luciferase activity in C3H10T1/2 cells. (**B**) 6xOSE2-luciferase activity was determined in C3H10T1/2 cells cotransfected with RUNX2, YAP, and TEAD4. (**C**) Schematic illustration of TEAD4 and TEAD4^{Y429H} mutation. (**D**) 3xSd-luciferase activity was determined in HEK-293T cells cotransfected with YAP, TEAD4, and TEAD4^{Y429H}. (**E**) Coimmunoprecipitation experiments of RUNX2, TEAD4, and TEAD4^{Y429H} in HEK-293T cells. The arrow indicated IgG heavy chain. (**F**) Effects of TEAD4 on RUNX2-activated 6xOSE2-luciferase activity in C3H10T1/2 cells. (**G**) Effects of TEAD4^{Y429H} on RUNX2-activated 6xOSE2-luciferase activity in C3H10T1/2 cells. (**H**) Cells isolated from WT mice were infected with GFP or TEAD shRNAs, TEAD4, or TEAD4^{Y429H} lentivirus. Osteoblast differentiation was evaluated by Alp staining and Alizarin red staining after culture in osteoblast differentiation medium for 7 days (top) and 14 days (bottom). Data are representative of three independent experiments. Scale bars, 3 mm. (**I**) Alp activity quantification was measured by phosphatase substrate assay ($n = 3$). (**J**) Relative mRNA levels of *Runx2*, *Alp*, *Col1α1*, *Osterix*, *Tead1*, and *Yap* were quantified by RT-PCR. In (A), (B), (D), (F), (G), (I), and (J), data were presented as means ± SEM; *$P < 0.05$, **$P < 0.01$, and ***$P < 0.001$; ns, no significance; unpaired Student's *t* test.

of the RUNX2-TEAD complex to some extent. Structural information may be required to answer this question and may provide more insights into the mechanism of VGLL4 in osteogenic differentiation.

Previous studies showed that mutations in RUNX2 cause CCD and *Runx2*$^{+/-}$ mice show a CCD-like phenotype. However, many patients with CCD do not have RUNX2 mutations. Our study may provide clues to the pathogenesis of these patients. A significant reduction of bone mass was observed in the adult mice, suggesting that VGLL4 and TEADs might be drug targets for treatment of cranial closure disorders and osteoporosis. In addition, further investigation of the clinical correlation of VGLL4 and cleidocranial dysplasia in a larger cohort will provide more accurate information for bone research. Our work also provides clues to researchers who are studying the roles of VGLL4 in tumors or other diseases. RUNX2 is highly expressed in breast and prostate cancer cells. RUNX2 contributes to tumor growth in bone and the accompanying osteolytic diseases (*32*). The regulation of RUNX2 transcriptional activity by TEADs and VGLL4 is likely to play essential roles in tumor, bone metastasis, and osteolytic diseases. Our work may provide clues to researchers who are studying the role of VGLL4 in bone tumors.

We demonstrate that TEADs are involved in regulating osteoblast differentiation by overexpressing and knocking down the TEAD family in vitro. However, the exact roles of TEADs in vivo need to be further confirmed by generation of TEAD1/2/3/4

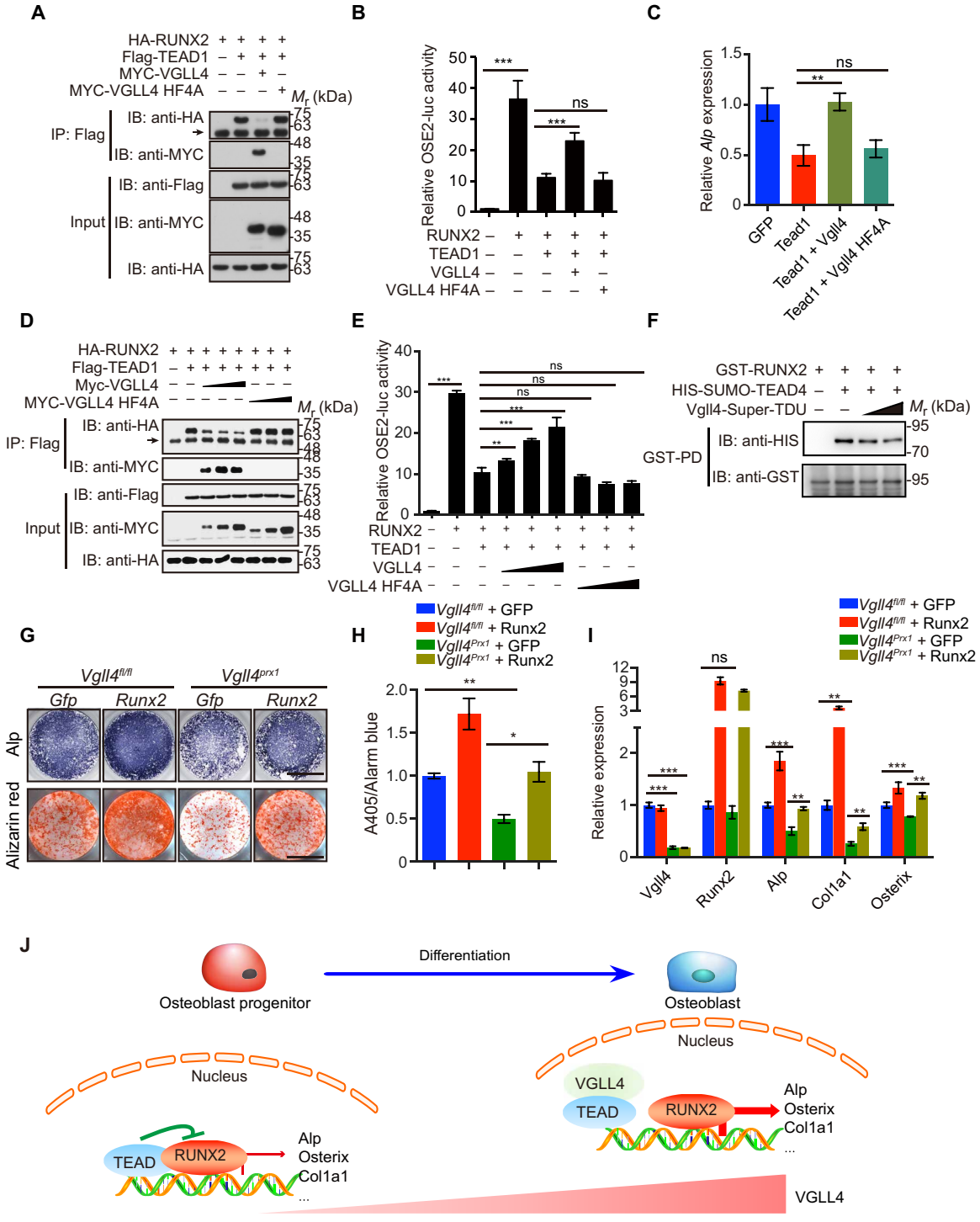

Fig. 6. RUNX2 rescues *Vgll4* deletion–mediated inhibition of osteogenesis differentiation. (**A**) Coimmunoprecipitation experiments of RUNX2, TEAD1, VGLL4, and VGLL4 HF4A in HEK-293T cells. The arrow indicated IgG heavy chain. (**B**) 6xOSE2-luciferase activity was determined in C3H10T1/2 cells cotransfected with RUNX2, VGLL4, VGLL4 HF4A, and TEAD1 ($n = 3$). (**C**) RT-PCR analysis of *Alp* expression in calvarial cells. Cells isolated from WT mice were infected with GFP, TEAD1, VGLL4, or VGLL4 HF4A lentivirus. (**D**) Coimmunoprecipitation experiments of RUNX2, TEAD1, and an increasing amount of VGLL4 or VGLL4 HF4A in HEK-293T cells. The arrow indicated IgG heavy chain. (**E**) 6xOSE2-luciferase activity was determined in C3H10T1/2 cells cotransfected with RUNX2, TEAD1, and an increasing amount of VGLL4 or VGLL4 HF4A. (**F**) Competitive GST pull-down assay to detect the effect of VGLL4 Super-TDU on the interaction between RUNX2 and TEAD4. (**G**) Cells isolated from *Vgll4*$^{fl/fl}$ and *Vgll4*^{prx1} mice were infected with GFP and RUNX2 lentivirus. Osteoblast differentiation was evaluated by Alp staining and Alizarin red staining after culture in osteoblast differentiation medium for 7 days (top) and 14 days (bottom). Data are representative of three independent experiments. Scale bars, 3 mm. (**H**) Alp activity quantification was measured by phosphatase substrate assay ($n = 3$). (**I**) Relative mRNA levels of *Vgll4*, *Runx2*, *Alp*, *Col1α1*, and *Osterix* were quantified by RT-PCR. (**J**) Schematic model of VGLL4/TEADs/RUNX2 in regulating osteogenic differentiation. In (B), (C), (E), (H), and (I), data were presented as means ± SEM; $^*P < 0.05$, $^{**}P < 0.01$, and $^{***}P < 0.001$; ns, no significance; unpaired Student's *t* test.

conditional knockout mice. In the follow-up work, we will continue to study the mechanism of TEADs in skeletal development and bone diseases. Overall, although there are still some shortcomings, our work has greatly contributed to understand the TEADs' regulation of RUNX2 activity.

Our work defines the role of VGLL4 in regulating osteoblast differentiation and bone development, and identifies that TEADs function as repressors of RUNX2 to inhibit osteoblast differentiation. We propose a model that VGLL4 dissociates the combination between TEADs and RUNX2. It is not clear whether VGLL4 is also involved in regulating other transcription factors or signaling pathways in the process of osteoblast differentiation and bone development. If that is the case, how to achieve cooperation will be another interesting issue worthy of further study.

METHODS

Mouse lines

Vgll4$^{Lacz/+}$ mice, *Vgll4* knockout (*Vgll4*$^{-/-}$) mice, *Vgll4*$^{Vgll4\text{-}eGFP/+}$ mice, and *Vgll4* conditional knockout (*Vgll4*$^{fl/fl}$) mice were generated as previously described (*16*, *17*), and *Vgll4*$^{fl/fl}$ mice were crossed with the *Prx1*-Cre and *Osx*-Cre strain to generate *Vgll4*^{prx1} and *Vgll4*^{Osx} mice. All mice analyzed were maintained on the C57BL/6 background. All mice were monitored in a specific pathogen–free environment and treated in strict accordance with protocols approved by the Shanghai Institute of Biochemistry and Cell Biology, Shanghai Institutes for Biological Sciences, Chinese Academy of Sciences.

Antibodies

The following antibodies were used: anti-Osterix antibody (1:1000; Santa Cruz Biotechnology, SC133871), anti-RUNX2 antibodies (1:1000; Santa Cruz Biotechnology, SC-390351 and SC-10758), anti-Flag antibody (1:5000; Sigma-Aldrich, F-3165), anti-HA (hemagglutinin) antibody (1:2000; Santa Cruz Biotechnology, SC-7392), anti-HA antibody (1:1000; Sangon Biotech, D110004), anti-MYC antibody (1:1000; ABclonal Technology, AE010), anti-PCNA antibody (1:1000; Santa Cruz Biotechnology, SC-56), rabbit immunoglobulin G (IgG) (Santa Cruz Biotechnology, SC-2027), mouse IgG (Sigma-Aldrich, I5381), anti-VGLL4 antibody (1:1000; ABclonal, A18248), anti-TEAD1 antibody (1:1000; ABclonal, A6768), anti-TEAD2 antibody (1:1000; ABclonal, A15594), anti-TEAD3 antibody (1:1000; ABclonal, A7454), anti-TEAD4 antibody (1:1000; Abcam, ab58310), and anti–pan-TEAD (1:1000; Cell Signaling Technology, 13295).

Cell culture

Cells were cultured at 37°C in humidified incubators containing an atmosphere of 5% CO_2. Human embryonic kidney (HEK)–293T cells were maintained in Dulbecco's Modified Eagle Medium (DMEM) (Corning, Corning, NY) supplemented with 10% fetal bovine serum (FBS) and 1% penicillin/streptomycin (Gibco) solution. C3H10T1/2 cells were maintained in α-minimum essential medium (α-MEM) (Corning, Corning, NY) supplemented with 10% FBS and 1% penicillin/streptomycin (Gibco) solution. To induce differentiation of BMSC into osteoblasts, cells were cultured in α-MEM containing 10% FBS, L-ascorbic acid (50 μg/ml), and β-glycerophosphate (1080 mg/ml). The osteoblast differentiation level assay was performed following a previously published method (*33*). To quantitate Alp activity, cells incubated with Alamar Blue to calculate cell numbers and then incubated with phosphatase substrate (Sigma-Aldrich, St. Louis, MO) dissolved in 6.5 mM Na_2CO_3, 18.5 mM $NaHCO_3$, and 2 mM $MgCl_2$ after washing by phosphate-buffered saline (PBS). Alp activity was then read with a luminometer (Envision). Bone nodule formation was stained with Alizarin red S solution (1 mg/ml; pH 5.5) after 14 days of induction.

Isolation of mouse BMSCs

We collected femurs and tibias from mice and flushed out the bone marrow cells with 10% FBS in PBS. All nuclear cells were seeded (2×10^6 cells per dish) in 100-mm culture dishes (Corning) and incubated at 37°C under 5% CO_2 conditions. After 48 hours, nonadherent cells were washed by PBS and adherent cells were cultured in α-MEM (Corning, Corning, NY) supplemented with 10% FBS and 1% penicillin/streptomycin (Gibco) solution for an additional 5 days. Mouse BMSCs in passage one were used in this study.

Real-time RT-PCR analysis

Total RNA was isolated from cells with TRIzol reagent (T9424, Sigma-Aldrich), and first-strand complementary DNA (cDNA) was synthesized from 0.5 μg of total RNA using the PrimeScript RT Reagent Kit (PR037A, TaKaRa). The real-time RT-PCR was performed with the Bio-Rad CFX96 System. Gene expression analysis from RT-PCR was quantified relative to Hprt.

Transient transfection and luciferase reporter assay

C3H10T1/2 cells were seeded overnight at 1×10^5 cells per well into a 12-well plate and transfected by PEI (polyethylenimine linear) with a luciferase reporter plasmid along with various expression constructs, as indicated. All wells were supplemented with control empty expression vector plasmids to keep the total amount of DNA constant. At 36 to 48 hours after transfection, the cells were harvested and subjected to dual-luciferase reporter assays according to the manufacturer's protocol (Promega).

Immunoprecipitation and immunoblotting

293T cells were seeded at 1×10^7 cells per 10-cm dish and cultured overnight. At 36 to 48 hours after transfection with PEI, cells were harvested and washed with cold PBS following experimental treatments. Then, cells were lysed with EBC buffer [50 mM tris (pH 7.5), 120 mM NaCl, and 0.5% NP-40] containing protease inhibitor cocktail (1:100; MedChem Express, HY-K0010). After ultrasonication, lysates were subjected to immunoprecipitation with anti-Flag antibodies (M2, Sigma-Aldrich) at 4°C overnight, followed by washing in lysis buffer, SDS–polyacrylamide gel electrophoresis (PAGE), and immunoblotting with the indicated antibody.

Protein purification and GST pull-down assay

RUNX2 and TEAD4-YBD were cloned into pGEX-4T-1-GST vector and expressed in *Escherichia coli* BL21 (DE3) cells. TEAD4 and TEAD4-TEA were cloned into HT-pET-28a-HIS-SUMO vector and expressed in *E. coli* BL21 (DE3) cells. The two TDU domains of VGLL4 were cloned into HT-pET-28a-MBP vector and expressed in *E. coli* BL21 (DE3) cells. VGLL4 Super-TDU was designed as previously described (*15*). GST, HIS-SUMO, and MBP-fused proteins were purified by affinity chromatography as previously described (*17*). The input and output samples were loaded to SDS-PAGE and detected by Western blotting.

Analysis of bone formation rate by calcein–Alizarin red S labeling

Calcein–Alizarin red S labeling measuring bone formation rate was performed as previously described (*33*).

μ-QCT analysis

Preparation of skeletal tissue and μ-QCT analysis were performed as previously described (*34*). The mouse femurs isolated from age- and sex-matched mice were skinned and fixed in 70% ethanol. Scanning was performed with the μ-QCT SkyScan 1176 System (Bruker Biospin). The mouse femurs were scanned at a 9-μm resolution for quantitative analysis. Three-dimensional (3D) images were reconstructed using a fixed threshold.

ChIP assay

ChIP experiments were carried out in BMSCs according to a standard protocol. The cell lysate was sonicated for 20 min (30 s on, 30 s off), and chromatin was divided into fragments ranging mainly from 200 to 500 base pairs in length. Immunoprecipitation was then performed using antibodies against TEAD4 (Abcam, ab58310), RUNX2 (Santa Cruz Biotechnology, SC-10758), and normal IgG. The DNA immunoprecipitated by the antibodies was detected by RT-PCR. The primers used were as follows: Alp-OSE2-ChIP-qPCR-F (5′-GTCTCCTGCCTGTGTTTCCACAGTG-3′), Alp-OSE2-ChIP-qPCR-R (5′-GAAGACGCCTGCTCTGTGGACTAGAG-3′), Alp-TBS-ChIP-qPCR-F (5′-CCTTGCATGTAAATGGTGGACATGG-3′), Alp-TBS-ChIP-qPCR-R (5′-TATCATAGTCACTGAGCACTCTCTTG-CG-3′), Osx-OSE2-ChIP-qPCR-F (5′-TTAACTGCCAAGCCATC-GCTCAAG-3′), Osx-OSE2-ChIP-qPCR-R (5′-CCTCTATGTGT-GTATGTGTGTTTACCAAACATC-3′), Osx-TBS-ChIP-qPCR-F (5′-ATGCCAAGAGATCCCTCATTAGGGAC-3′), Osx-TBS-ChIP-qPCR-R (5′-AGCTTGGTGAGCACAGCAAAGACAC-3′), Col1a1-TBS/OSE2-Chip-qPCR-F (5′-CTCAGCCTCAGAGCTGTTATTTATT-AGAAAGG-3′), and Col1a1-TBS/OSE2-Chip-qPCR-R (5′-TTA-ATCTGATTAGAACCTATCAGCTAAGCAGATG-3′). TBS indicated TEAD binding sites.

RNA interference

Mouse TEAD1, TEAD2, TEAD3, and TEAD4 siRNAs and the control siRNA were synthesized from Shanghai Gene Pharma Co. Ltd., Shanghai, China. siRNA oligonucleotides were transfected in C3H10T1/2 by Lipofectamine RNAiMAX (Invitrogen) following the manufacturer's instructions. Two pairs of siRNAs were used to perform experiments.

Histology and immunofluorescence

Hematoxylin and eosin stain and immunohistochemistry were performed as previously described (*7*). Tissue sections were used for TRAP staining according to the standard protocol. Tissues were fixed in 4% paraformaldehyde for 48 hours and incubated in 15% DEPC (diethyl pyrocarbonate)–EDTA (pH 7.8) for decalcification. Then, specimens were embedded in paraffin and sectioned at 7 μm. Immunofluorescence was performed as previously described (*33*). Sections were blocked in PBS with 10% horse serum and 0.1% Triton for 1 hour and then stained overnight with anti-PCNA antibody (SC-56). Donkey anti-rabbit Alexa Fluor 488 (1:1000; Molecular Probes, A21206) was used as secondary antibodies. DAPI (4′,6-diamidino-2-phenylindole) (Sigma-Aldrich, D8417) was used for counterstaining. Slides were mounted with anti-fluorescence mounting medium (Dako, S3023), and images were acquired with a Leica SP5 and SP8 confocal microscope. For embryonic mice, 5-mm tissue sections were used for immunohistochemistry staining, DIG-labeled in situ hybridization (Roche), and immunohistochemical staining (Dako).

TUNEL staining

TUNEL staining for apoptosis testing was performed as provided by Promega (G3250).

MTT assay

MTT assay for cell viability was performed as provided by Thermo Fisher Scientific.

Measurement of PINP and CTX-1 concentrations

We determined serum concentrations of PINP using the Mouse PINP EIA Kit (YX-160930M) according to the instructions provided. In addition, we determined serum concentrations of CTX-1 using the Mouse CTX-1 EIA Kit (YX-032033M) according to the instructions provided.

SO staining

Tissue sections were used for SO staining according to the standard protocol. After paraffin sections were dewaxed into water, they were acidified with 1% acetic acid for 10 s and then fast green for 2 min, acidified with 1% acetic acid for 10 s, stained with SO for 3 min and 95% ethanol for 5 s, and dried and sealed with neutral glue.

Statistics

Statistical analysis was performed by unpaired, two-tailed Student's *t* test for comparison between two groups using GraphPad Prism Software. A P value of less than 0.05 was considered statistically significant.

SUPPLEMENTARY MATERIALS

Supplementary material for this article is available at http://advances.sciencemag.org/cgi/content/full/6/43/eaba4147/DC1

View/request a protocol for this paper from *Bio-protocol*.

REFERENCES AND NOTES

1. N. Suda, M. Hattori, K. Kosaki, A. Banshodani, K. Kozai, K. Tanimoto, K. Moriyama, Correlation between genotype and supernumerary tooth formation in cleidocranial dysplasia. *Orthod. Craniofac. Res.* **13**, 197–202 (2010).
2. S. Mundlos, F. Otto, C. Mundlos, J. B. Mulliken, A. S. Aylsworth, S. Albright, D. Lindhout, W. G. Cole, W. Henn, J. H. Knoll, M. J. Owen, R. Mertelsmann, B. U. Zabel, B. R. Olsen, Mutations involving the transcription factor CBFA1 cause cleidocranial dysplasia. *Cell* **89**, 773–779 (1997).
3. T. Komori, H. Yagi, S. Nomura, A. Yamaguchi, K. Sasaki, K. Deguchi, Y. Shimizu, R. T. Bronson, Y. H. Gao, M. Inada, M. Sato, R. Okamoto, Y. Kitamura, S. Yoshiki, T. Kishimoto, Targeted disruption of *Cbfa1* results in a complete lack of bone formation owing to maturational arrest of osteoblasts. *Cell* **89**, 755–764 (1997).
4. F. Otto, A. P. Thornell, T. Crompton, A. Denzel, K. C. Gilmour, I. R. Rosewell, G. W. Stamp, R. S. Beddington, S. Mundlos, B. R. Olsen, P. B. Selby, M. J. Owen, *Cbfa1*, a candidate gene for cleidocranial dysplasia syndrome, is essential for osteoblast differentiation and bone development. *Cell* **89**, 765–771 (1997).
5. P. Ducy, R. Zhang, V. Geoffroy, A. L. Ridall, G. Karsenty, Osf2/Cbfa1: A transcriptional activator of osteoblast differentiation. *Cell* **89**, 747–754 (1997).
6. Z. Liu, X. Yao, G. Yan, Y. Xu, J. Yan, W. Zou, G. Wang, Mediator MED23 cooperates with RUNX2 to drive osteoblast differentiation and bone development. *Nat. Commun.* **7**, 11149 (2016).
7. Q. Dai, Z. Xu, X. Ma, N. Niu, S. Zhou, F. Xie, L. Jiang, J. Wang, W. Zou, mTOR/Raptor signaling is critical for skeletogenesis in mice through the regulation of Runx2 expression. *Cell Death Differ.* **24**, 1886–1899 (2017).

8. B. Zhao, Q.-Y. Lei, K.-L. Guan, The Hippo–YAP pathway: New connections between regulation of organ size and cancer. *Curr. Opin. Cell Biol.* **20**, 638–646 (2008).
9. W. Zhang, Y. Gao, P. Li, Z. Shi, T. Guo, F. Li, X. Han, Y. Feng, C. Zheng, Z. Wang, F. Li, H. Chen, Z. Zhou, L. Zhang, H. Ji, VGLL4 functions as a new tumor suppressor in lung cancer by negatively regulating the YAP-TEAD transcriptional complex. *Cell Res.* **24**, 331–343 (2014).
10. M.-X. Yin, L. Zhang, Hippo signaling in epithelial stem cells. *Acta Biochim. Biophys. Sin.* **47**, 39–45 (2015).
11. B. Zhao, X. Ye, J. Yu, L. Li, W. Li, S. Li, J. Yu, J. D. Lin, C.-Y. Wang, A. M. Chinnaiyan, Z.-C. Lai, K.-L. Guan, TEAD mediates YAP-dependent gene induction and growth control. *Genes Dev.* **22**, 1962–1971 (2008).
12. Y. Deng, A. Wu, P. Li, G. Li, L. Qin, H. Song, K. K. Mak, Yap1 regulates multiple steps of chondrocyte differentiation during skeletal development and bone repair. *Cell Rep.* **14**, 2224–2237 (2016).
13. J.-X. Pan, L. Xiong, K. Zhao, P. Zeng, B. Wang, F.-L. Tang, D. Sun, H.-h. Guo, X. Yang, S. Cui, W.-F. Xia, L. Mei, W.-C. Xiong, YAP promotes osteogenesis and suppresses adipogenic differentiation by regulating β-catenin signaling. *Bone Res.* **6**, 18 (2018).
14. H.-H. Chen, S. J. Mullett, A. F. Stewart, Vgl-4, a novel member of the vestigial-like family of transcription cofactors, regulates alpha1-adrenergic activation of gene expression in cardiac myocytes. *J. Biol. Chem.* **279**, 30800–30806 (2004).
15. S. Jiao, H. Wang, Z. Shi, A. Dong, W. Zhang, X. Song, F. He, Y. Wang, Z. Zhang, W. Wang, X. Wang, T. Guo, P. Li, Y. Zhao, H. Ji, L. Zhang, Z. Zhou, A peptide mimicking VGLL4 function acts as a YAP antagonist therapy against gastric cancer. *Cancer Cell* **25**, 166–180 (2014).
16. W. Yu, X. Ma, J. Xu, A. W. Heumüller, Z. Fei, X. Feng, X. Wang, K. Liu, J. Li, G. Cui, G. Peng, H. Ji, J. Li, N. Jing, H. Song, Z. Lin, Y. Zhao, Z. Wang, B. Zhou, L. Zhang, VGLL4 plays a critical role in heart valve development and homeostasis. *PLOS Genet.* **15**, e1007977 (2019).
17. X. Feng, Z. Wang, F. Wang, T. Lu, J. Xu, X. Ma, J. Li, L. He, W. Zhang, S. Li, W. Yang, S. Zhang, G. Ge, Y. Zhao, P. Hu, L. Zhang, Dual function of VGLL4 in muscle regeneration. *EMBO J.* **38**, e101051 (2019).
18. M. Logan, J. F. Martin, A. Nagy, C. Lobe, E. N. Olson, C. J. Tabin, Expression of Cre recombinase in the developing mouse limb bud driven by a *Prxl* enhancer. *Genesis* **33**, 77–80 (2002).
19. W.-M. Woo, H. H. Zhen, A. E. Oro, Shh maintains dermal papilla identity and hair morphogenesis via a Noggin–Shh regulatory loop. *Genes Dev.* **26**, 1235–1246 (2012).
20. S. J. Rodda, A. P. McMahon, Distinct roles for Hedgehog and canonical Wnt signaling in specification, differentiation and maintenance of osteoblast progenitors. *Development* **133**, 3231–3244 (2006).
21. S. Joshi, G. Davidson, S. Le Gras, S. Watanabe, T. Braun, G. Mengus, I. Davidson, TEAD transcription factors are required for normal primary myoblast differentiation in vitro and muscle regeneration in vivo. *PLOS Genet.* **13**, e1006600 (2017).
22. X. Yang, K. Matsuda, P. Bialek, S. Jacquot, H. C. Masuoka, T. Schinke, L. Li, S. Brancorsini, P. Sassone-Corsi, T. M. Townes, A. Hanauer, G. Karsenty, ATF4 is a substrate of RSK2 and an essential regulator of osteoblast biology; implication for Coffin-Lowry syndrome. *Cell* **117**, 387–398 (2004).
23. Z. Li, B. Zhao, P. Wang, F. Chen, Z. Dong, H. Yang, K.-L. Guan, Y. Xu, Structural insights into the YAP and TEAD complex. *Genes Dev.* **24**, 235–240 (2010).
24. Y. Tang, T. Feinberg, E. T. Keller, X.-Y. Li, S. J. Weiss, Snail/Slug binding interactions with YAP/TAZ control skeletal stem cell self-renewal and differentiation. *Nat. Cell Biol.* **18**, 917–929 (2016).
25. Y. Liu, G. Wang, Y. Yang, Z. Mei, Z. Liang, A. Cui, T. Wu, C.-Y. Liu, L. Cui, Increased TEAD4 expression and nuclear localization in colorectal cancer promote epithelial–mesenchymal transition and metastasis in a YAP-independent manner. *Oncogene* **35**, 2789–2800 (2016).
26. G. Karsenty, E. F. Wagner, Reaching a genetic and molecular understanding of skeletal development. *Dev. Cell* **2**, 389–406 (2002).
27. G. Yang, L. Zhu, N. Hou, Y. Lan, X.-M. Wu, B. Zhou, Y. Teng, X. Yang, Osteogenic fate of hypertrophic chondrocytes. *Cell Res.* **24**, 1266–1269 (2014).
28. L. Yang, K. Y. Tsang, H. C. Tang, D. Chan, K. S. Cheah, Hypertrophic chondrocytes can become osteoblasts and osteocytes in endochondral bone formation. *Proc. Natl. Acad. Sci. U.S.A.* **111**, 12097–12102 (2014).
29. Y. Matsumoto, J. La Rose, O. A. Kent, M. J. Wagner, M. Narimatsu, A. D. Levy, M. H. Omar, J. Tong, J. R. Krieger, E. Riggs, Y. Storozhuk, J. Pasquale, M. Ventura, B. Yeganeh, M. Post, M. F. Moran, M. D. Grynpas, J. L. Wrana, G. Superti-Furga, A. J. Koleske, A. M. Pendergast, R. Rottapel, Reciprocal stabilization of ABL and TAZ regulates osteoblastogenesis through transcription factor RUNX2. *J. Clin. Invest.* **126**, 4482–4496 (2016).
30. D. Lai, K. C. Ho, Y. Hao, X. Yang, Taxol resistance in breast cancer cells is mediated by the hippo pathway component TAZ and its downstream transcriptional targets Cyr61 and CTGF. *Cancer Res.* **71**, 2728–2738 (2011).
31. D. Lai, X. Yang, BMP4 is a novel transcriptional target and mediator of mammary cell migration downstream of the Hippo pathway component TAZ. *Cell. Signal.* **25**, 1720–1728 (2013).
32. J. Pratap, J. B. Lian, A. Javed, G. L. Barnes, A. J. van Wijnen, J. L. Stein, G. S. Stein, Regulatory roles of Runx2 in metastatic tumor and cancer cell interactions with bone. *Cancer Metastasis Rev.* **25**, 589–600 (2006).
33. L. Wang, N. Niu, L. Li, R. Shao, H. Ouyang, W. Zou, H3K36 trimethylation mediated by SETD2 regulates the fate of bone marrow mesenchymal stem cells. *PLOS Biol.* **16**, e2006522 (2018).
34. M. B. Greenblatt, J.-H. Shim, W. Zou, D. Sitara, M. Schweitzer, D. Hu, S. Lotinun, Y. Sano, R. Baron, J. M. Park, S. Arthur, M. Xie, M. D. Schneider, B. Zhai, S. Gygi, R. Davis, L. H. Glimcher, The p38 MAPK pathway is essential for skeletogenesis and bone homeostasis in mice. *J. Clin. Invest.* **120**, 2457–2473 (2010).

Acknowledgments: We thank A. McMahon (Harvard University, Boston, MA) for providing the Prx1-Cre mouse line. We thank the cell biology core facility and the animal core facility of Shanghai Institute of Biochemistry and Cell Biology for assistance. **Funding:** This work was supported by the National Natural Science Foundation of China (nos. 81725010, 31625017, 81672119, and 31530043), National Key Research and Development Program of China (2017YFA0103601 and 2019YFA0802001), "Strategic Priority Research Program" of Chinese Academy of Sciences (XDB19000000), Shanghai Leading Talents Program, Science and Technology Commission of Shanghai Municipality (19ZR1466300), and Youth Innovation Promotion Association CAS (2018004). **Author contributions:** Z.W., L.Z., and W.Z. conceived and supervised the study. J.S. conceived and designed the study, performed the experiments, analyzed the data, and wrote the manuscript. X.F. made the constructs, performed the in vitro pull-down assay and ChIP experiments, analyzed the data, and revised the manuscript. L.Z. and Z.W. provided genetic strains of mice. J.S. and Z.W. bred and analyzed *Vgll4*$^{-/-}$ mice. J.L. and J.W. cultured the cells and made the constructs. W.Z., L.Z., X.F., and Z.W. edited the manuscript. **Competing interests:** The authors declare that they have no competing interests. **Data and materials availability:** All data needed to evaluate the conclusions in the paper are present in the paper and/or the Supplementary Materials. Additional data related to this paper may be requested from the authors.

Submitted 2 December 2019
Accepted 8 September 2020
Published 23 October 2020
10.1126/sciadv.aba4147

Citation: J. Suo, X. Feng, J. Li, J. Wang, Z. Wang, L. Zhang, W. Zou, VGLL4 promotes osteoblast differentiation by antagonizing TEADs-inhibited Runx2 transcription. *Sci. Adv.* **6**, eaba4147 (2020).